Open Access

Catalysis Research

LIDSEN Publishing Inc.

Original Research

Rapid Degradation of Tartrazine Yellow Dye by Photo-Fenton Action at the Interface of Magnetite and Silica Nanoparticles

Bianca Gonçalves Rodrigues [1, †], Elaine Alves de Faria Braga [2, †], Marccus Victor Almeida Martins [3, *], Jocélia Pereira de Carvalho Oliveira [4, *]

1. Instituto de Química, Universidade Federal de Catalão, Goiás, Brazil; E-Mail: rodriguesbianca68@gmail.com
2. Instituto Federal de Goiás, Inhumas, Goiás, Brazil; E-Mail: elaine.faria@ifg.edu.br
3. Instituto Federal Goiano, Catalão, Goiás, Brazil; E-Mail: marccus.victor@ifgoiano.edu.br
4. Instituto de Química, Universidade Federal de Catalão, Goiás, Brazil; E-Mail: joceliapereira@ufcat.edu.br

† These authors contributed equally to this work.

* **Correspondences:** Marccus Victor Almeida Martins and Jocélia Pereira de Carvalho Oliveira; E-Mails: marccus.victor@ifgoiano.edu.br; joceliapereira@ufcat.edu.br

Academic Editor: Narendra Kumar

Catalysis Research
2026, volume 6, issue 2
doi:10.21926/cr.2602005

Received: February 14, 2026
Accepted: June 01, 2026
Published: June 07, 2026

Abstract

This study reports the synthesis of magnetic nanoparticles (Fe_3O_4) supported on silica (SiO_2), obtained from the chemical and thermal treatment of coconut mesocarp. The spectroscopic and morphological properties of this nanocomposite composed of magnetite and silica (Np-Fe_3O_4/SiO_2) were investigated using Infrared (FTIR), Ultraviolet and Visible (UV-Vis), X-ray Diffraction (XRD), Field Emission Scanning Electron Microscopy (FEG-SEM), and Energy Dispersive X-ray Spectroscopy (EDS) techniques. The synthesized material was applied in heterogeneous catalytic reactions to photodegrade the tartrazine yellow dye in the presence of hydrogen peroxide (Fenton reaction). FTIR spectra showed that treatment in a basic medium (NaOH) promotes the rupture of lignocellulosic fiber units, thereby decreasing the intensity of the chemical bonds. Heat treatment at 800°C generates silica, confirmed by

the presence of the Si–O–Si band stretching vibration. Morphologically, the generated silica presented a random geometry, with particles larger than 10 µm filled with pores. The magnetite synthesized by basic co-precipitation on the silica presented an average diameter of 10 nm, as confirmed by FEG-SEM images and the Scherrer equation. The photocatalytic performance of the Np-Fe_3O_4/SiO_2 was analyzed, achieving nearly 100% degradation of the tartrazine dye in 75 minutes of reaction in the presence of H_2O_2. In the absence of H_2O_2, the dye concentration decreases by only 18% over the same reaction time, probably due to saturation of the dye molecules at the nanocatalyst interface. The adsorption equilibrium parameters were investigated using the Langmuir adsorption isotherm model, which revealed that the adsorption capacity of the Np-Fe_3O_4/SiO_2 system is approximately twice that of the SiO_2 system: the maximum amount of dye adsorbed on the nanomaterial's (q_m) surface was 0.35 mg/g for SiO_2 and 0.79 mg/g for Fe_3O_4/SiO_2. This photodegradation efficiency is associated with an increase in the nanoparticle's surface area, which enhances the adsorption capacity for dye molecules. Furthermore, the excess radicals generated by the Fenton reaction also catalyze the degradation of the dye.

Keywords
Photodegradation; Fe_3O_4/SiO_2 nanoparticles; Photo-Fenton; heterojunction

1. Introduction

Water contamination by organic and inorganic substances is a critical problem for humanity. Various chemical substances pollute water reservoirs. These chemical substances originate from human activities, such as agricultural, textile, food processing, mining, and automotive industries. Given this problem, it is necessary to develop effective, efficient technologies to remove or reduce these pollutants in aquatic environments. In the field of chemistry, advanced oxidation processes (AOPs) [1] are widely used for their effectiveness and efficiency in removing or reducing organic pollutants from aqueous media.

Advanced Oxidation Processes technology is based on the generation of positive (holes) and negative (electrons) charges at the surface of a photoactivated material, which is usually a semiconductor [2, 3]. As the surface of a semiconductor material receives light, electrons e^- from the valence band are promoted to the conduction band, generating a hole with a positive charge (h^+) that specifically reacts with the chemical groups of certain organic pollutants.

Based on this process, several studies present creative alternatives to better control the generation of the (e^-/h^+) pair. For example, structural modification [4] (doping) of the classic semiconductor TiO_2 creates new electronic and optical properties that promote rapid degradation of pollutants. Within this same strategy, the intrinsic modification of zinc oxide with boron [5], g-C_3N_4 [6], Mg [7], and Al [8] has also been ingeniously reported as a way to enhance the photodegradation of pollutants in water.

Another widely reported strategy to increase the photodegradation of these pollutants is using materials with heterojunctions. Contact between two materials with distinct band gaps inhibits recombination of the (e^-/h^+) pair, thereby increasing the amount of charge on the semiconductor

surface for a longer time to react with the organic pollutant. Martins' co-workers [9] reported that the yellow dye tartrazine was more readily removed from water using a semiconductor heterojunction based on SiO_2 and Fe_3O_4. The same conclusion was also reported for other heterojunctions formed between ZnO/BiOI [10], $gC_3N_4/BiVO_4$ [11], and gC_3N_4/BiOCl [12].

Both doping and the creation of heterojunctions in photocatalytic materials are widely used for degradation. Dyes containing the azo group (N=N) are extensively studied due to their widespread use in the food and textile industries [13]. In general, these dyes have high molecular mass and complex chemical structures, making them difficult to biodegrade. The presence of these macromolecules in the environment leads to serious problems for animals living in aquatic biomes, as they can even accumulate in the human body, causing health damage.

Critically, the development of strategies for the efficient removal of dyes from aqueous media often relies on expensive materials and time-consuming syntheses. It is desirable that a photocatalyst material has the advantages of being a low-cost precursor material, easy and rapid synthesis, being reusable, photostable, and biologically inert [14].

To generate motive power, there has been much recent discussion about the global need to shift from fossil fuels to biomass-based energy generation. Given the projected large-scale use of various biomasses, the waste generated could become a global problem. For example, when improperly disposed of, waste from sugarcane, corn, green coconut, soy, and sorghum can cause environmental contamination. The proposal of physical and chemical treatment routes to add value to this waste stands out as a possible solution. The literature [15-17] reports several studies highlighting the potential of certain waste products as adsorbents for decontaminating aqueous systems.

Using biomass derived from lignocellulosic constituents is an interesting strategy for the decontamination of aquatic environments because it involves an environmentally friendly adsorbent. On the other hand, there are some disadvantages, mainly due to limitations compared to adsorbents that depend on specific chemical interactions. To overcome this limitation in adsorption specificity, some studies convert the organic matrix of biomass into inorganic matrices via calcination. In this context, the generation of a silica-based material from biomass waste converges on using a material that is generally discarded into the environment, transforming it into a value-added [18] material at zero cost. For example, Fatimah and co-workers [19] studied the photocatalytic performance of the TiO_2/SiO_2 composite, in which the silica was derived from bamboo leaves. Additionally, Hajam and co-workers [20] used wood sawdust residue as biomass to produce bioactive silica during the photodegradation of the methylene blue dye. Similarly, silica from rice husks [21-23] is also widely used for the photodegradation of organic pollutants.

The production and consumption of green coconuts worldwide are mostly concentrated in Asia. However, Brazil is often cited as a world leader in producing this fruit. Locally, the improper disposal of green coconut waste is an environmental problem. Therefore, this biomass can be, and is, used as a precursor biomaterial for silica for the photodegradation of organic pollutants. The husks [24], endocarp [25], and mesocarp of coconuts are good biomass residues capable of generating silica with photocatalytic properties.

Given the large amount of coconut produced and the waste generated in Brazil, it becomes very obvious to answer two questions: (i) How to reuse this biomass, seen as an environmental problem, to depollute aqueous systems from complex organic molecules? (ii) Why then use the silica generated from this biomass?

The answer to the first question lies in the theme of coconut waste sustainability. Developing a physicochemical route that is easy to process and uses conventional procedures, such as chemical and thermal treatments, imparts new properties in the biomass or biosilica, creating a chemically active material for the decontamination of effluents. In addition to being sustainable and environmentally friendly, this approach is a much more economically viable option than using precious-metal semiconductors, which makes photocatalyst production much more expensive.

To answer the second question, this study will explain the physicochemical properties of SiO_2 from the perspective of its application in the decontamination of effluents. Silicon is the second-most-abundant chemical element on Earth, second only to oxygen [26, 27]. Due to this abundance, it satisfies the need for non-exhaustible resources. Furthermore, regarding the formation of silicon oxide, it is classified as a semiconductor, exhibiting a band gap of approximately 9.0 eV [28, 29]. Since the difference between the valence band (VB) and the conduction band (CB) is the critical factor for photocatalytic applications, this difference makes SiO_2 an unfavorable material for photogenerating surface charges. However, with the different synthesis routes, the literature reports that doping and the formation of heterojunctions allow for easy adjustment of the band gap value to favor the formation of the e^-/h^+ pair.

Given the context of the two previous questions, this study reported the reuse of coconut mesocarp as a precursor biomass in the production of silica (SiO_2). This silica served as a support material for the rapid, easy co-precipitation of magnetite nanoparticles. The resulting composite nanomaterial (Np-Fe_3O_4/SiO_2) was used as a nanophotocatalyst in heterogeneous catalysis reactions to degrade tartrazine yellow dye molecules. The proposed material incorporates the principles of reusing coconut waste and magnetic nanomaterials, offering an efficient technology for the depollution of aquifer systems.

2. Materials and Methods

2.1 Obtaining Silica (SiO_2)

Figure 1 shows the coconut biomass collected from a street market located in the city center of Catalão, Goiás, Brazil. The mesocarp of this biomass was washed with distilled water to remove impurities and small insects. Then, the biomass was placed in an oven at 80°C for 24 h to remove excess water. Finally, the biomass fiber (Figure 1B) was crushed to obtain particulate material. This material underwent chemical treatment with a NaOH solution (2.0 mol L^{-1}) for 1 h. Then, it was washed with distilled water until the wash water reached neutral pH (pH = 7). After the treated and washed biomass was completely dried, it was burned in a muffle furnace at 800°C at a heating rate of 10°C/min for 1 h to obtain biomass ash, as presented in Figure 1C.

Figure 1 Photographs of (A) discarded coconut, (B) coconut fiber, and (C) ash obtained at a temperature of 800°C.

2.2 Synthesis of the Fe_3O_4/SiO_2 Nanoparticles

The synthesis of Fe_3O_4/SiO_2 nanoparticles used analytical-grade reagents without further purification. Ferric chloride ($FeCl_3$), ferrous chloride ($FeCl_2$), and ammonium hydroxide (NH_4OH) were purchased from Aldrich. Np-Fe_3O_4/SiO_2 was synthesized by the coprecipitation method with some modifications, as reported by Martins and co-workers [30]. First, the solutions were prepared using distilled water: 25 mL of $FeCl_2$ (1 mmol L^{-1}) and 50 mL of $FeCl_3$ (1 mmol L^{-1}). In a three-necked glass flask, 25 mL of $FeCl_2$ and 50 mL of $FeCl_3$ were added under constant stirring in a controlled atmosphere (N_2) at 50°C. Then, 150 µL of NH_4OH (7 mol L^{-1}) was added. Instantly, 50 mL of SiO_2 suspension (0.1 g L^{-1}) was added, followed by another 150 µL of NH_4OH. The system was turned off minutes after the solution had changed from yellow to black. After adding 150 µL of NH_4OH to the solution, the solution abruptly changed from yellow to black, typical of magnetite. Adding another 150 µL was necessary to ensure a complete supply of iron ions. This entire synthesis procedure lasted only 5 min.

2.3 Photodegradation of Tartrazine Yellow Dye

To ensure that the reaction reached adsorption equilibrium, the photocatalyst and dye were left in the dark for 30 minutes. After that, tests were performed with light. For photocatalytic degradation, a 50-ppm stock solution of tartrazine yellow dye was prepared in double-distilled water. Photodegradation experiments were carried out with a solution of 50 ppm of tartrazine yellow dye. First, 5 mg L^{-1} of Np-Fe_3O_4/SiO_2 was directly added to 100 mL of tartrazine yellow dye solution and placed in a photoreactor. Then, the mixture was placed under magnetic stirring and irradiated with UV light from a 125 W polychromatic mercury vapor lamp. The mixture was stirred for 1 h in the absence of light to promote adsorption of the tartrazine yellow dye onto the photocatalyst (considered time 0 in all graphs). After 1 h, the reactor lamp was turned on, and the reaction was conducted for 120 min. At 15-minute intervals, 3 mL of the solution was collected and analyzed using a UV-Vis spectrophotometer at 426 nm, the maximum absorbance of the azo group of tartrazine. An external magnetic field was applied to each aliquot removed to separate Np-Fe_3O_4/SiO_2 from the solution.

2.4 Characterizations of Np-Fe_3O_4/SiO_2

UV-Vis spectroscopy experiments were performed on a Varian spectrophotometer (Cary 50 scan) at 25°C (transmittance mode), over 200-800 nm, using a 1 cm quartz cuvette. The morphology and size of Np-Fe_3O_4/SiO_2 were analyzed in a field-emission gun scanning electron microscope (FEG-SEM), Jeol Brand, JSM-7100FT, using the secondary electrons. For the FEG-SEM analysis, a small amount of Np-Fe_3O_4/SiO_2 was dripped on carbon tape. Chemical mapping was performed using energy-dispersive X-ray spectroscopy (EDS) coupled to FEG-SEM. X-ray diffraction (XRD) analyses were performed on a Shimadzu XRD-6100 diffractometer operated at 30 kV and 30 mA, equipped with Cu-Kα radiation and a graphite monochromator, over a 5° to 85° range. Fourier transform infrared (FTIR) spectroscopy analysis was performed in a Cary 630 FTIR Spectrometer (Agilent) in attenuated total reflectance (ATR) mode, with a wavelength range between 4000 and 500 cm^{-1} and a resolution of 4 cm^{-1}.

2.5 Kinetic Parameters

The Langmuir adsorption isotherm model was used to model the adsorption equilibrium at the photocatalyst/dye interface, according to Equation 1.

$$\frac{C_e}{q_e} = \frac{1}{q_m \times K_L} + \frac{1}{q_m} \times C_e \quad (1)$$

where C_e is the tartrazine concentration in the equilibrium state (mg L^{-1}), q_e is the amount of dye that was adsorbed to equilibrium (mg g^{-1}), K_L is the equilibrium constant, and q_m is the maximum amount that can be adsorbed in the adsorption process. Langmuir constants (K_L and q_m) were determined by linear regression of the linearized equation. This model assumes that, at equilibrium, the number of sites adsorbed on the surface of nanoparticles is constant, and only one substrate is adsorbed at each site.

3. Results and Discussion

The transformation of coconut husk biomass from organic to inorganic was initially studied by infrared spectroscopy. Figure 2A shows the gradual reduction of this organic profile with the chemical (2 mol L^{-1} NaOH) and thermal (calcination at 800°C) steps. In the infrared spectrum of the natural fiber (green line), we can see vibrational bands associated with the main chromophores of lignin, cellulose, and hemicellulose, as Table 1 shows [31, 32]. When coconut fibers are subjected to chemical treatment (blue line) in a basic NaOH solution (2 mol L^{-1}), the stretching band of the C–O bond disappears [33] considerably, followed by a decrease in the intensity of the O–H bonds and in the aromatic region (800 cm^{-1}). These modifications in a basic medium indicate rupture of the plant cell wall [34], which is composed of the cellulosic units of coconut fiber, as similarly reported by Mulana and co-workers [35].

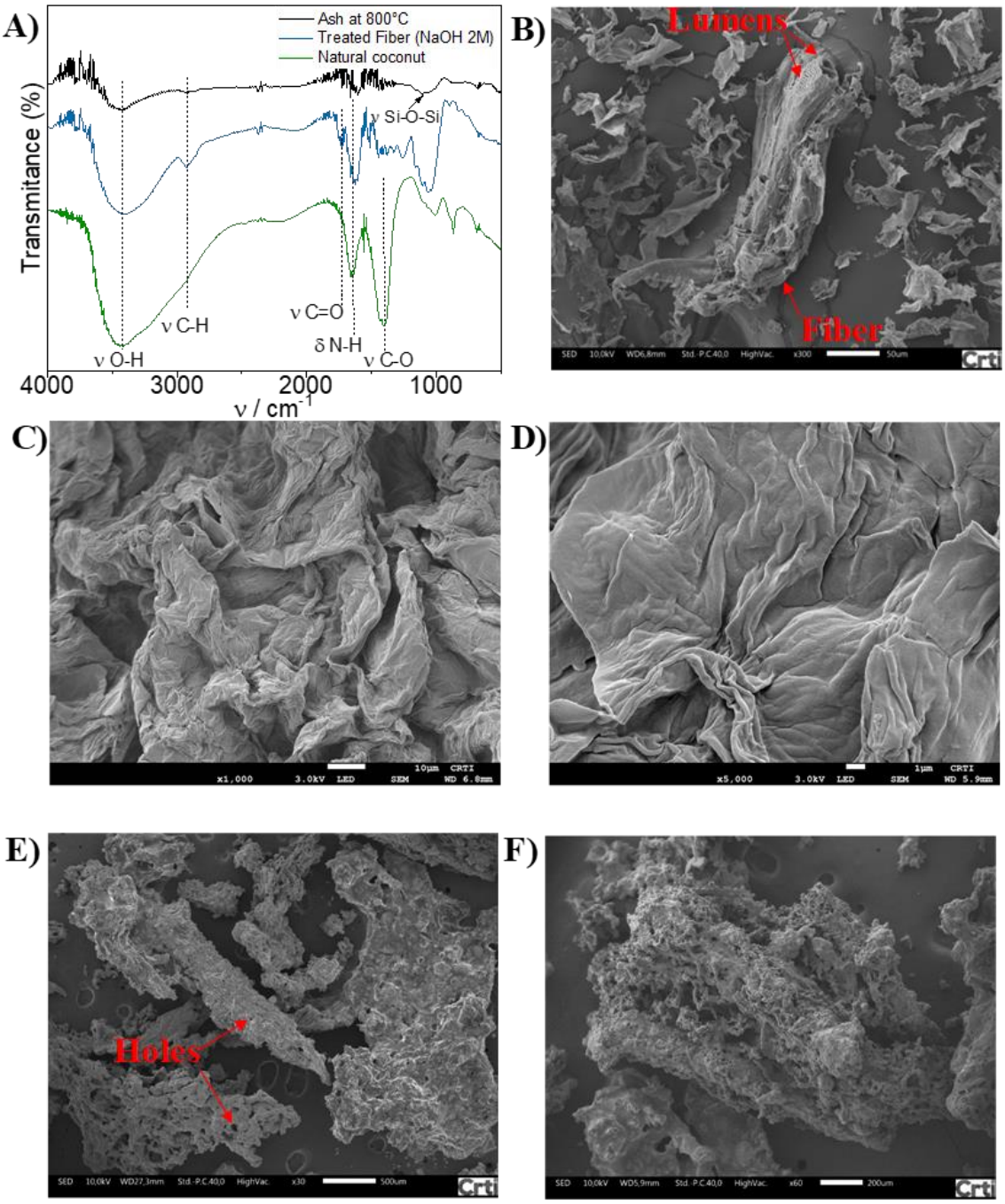

Figure 2 (A) FTIR spectra for natural coconut (green), NaOH-treated fiber (blue), and ash calcined at 800°C (black). FEG-SEM images for (B) natural fiber, (C) and (D) NaOH-treated fiber, and (E) and (F) ash calcined at 800°C.

Table 1 Chemical bonds and frequency of vibrational modes.

Chemical bond	Frequency (cm^{-1})
ν(O–H)	3425
ν(C–H)	2910
ν(C=O)	1725
δ(N–H)	1640
ν(C–O)	1410

Complete modification of coconut fiber is achieved by subjecting the fiber treated in a basic medium to calcination at a temperature of 800°C for 1 hour in a muffle furnace (black line). Virtually all vibrational modes associated with lignin, cellulose, and hemicellulose disappear. In addition, the band associated with the silicate group (Si–O–Si) appears at 1060 cm^{-1} [36], indicating the formation of silica.

It is also possible to track the morphological changes generated by chemical and thermal treatment of the fiber using FEG-SEM. The FEG-SEM image in Figure 2B shows fibers with lumens arranged in parallel, typical of fibers under natural conditions, as also discussed by Armad and co-workers [37]. However, these plant structures disappear upon treatment in a basic medium, leaving structures with flatter and smoother profiles (Figure 2C and Figure 2D). This proves that the basic medium breaks down cell walls and deconstructs the cellulosic units, as evidenced by FTIR. After calcination, the material consists of smaller micrometric particles and a random geometry with numerous scattered pores [9]. The images show silica particles with an average size ranging from 500 nm to 1 mm. These characteristics indicate the formation of silica (SiO_2), as can be seen in Figure 2E and Figure 2F, as similarly reported by Sarker and co-workers [38].

Chemical mapping of the natural fiber and silica was performed using EDS. By focusing the energy beam on point P2 in Figure 3A, corresponding to the natural fiber, the energy (in eV) of the chemical elements C, O, Al, and Si appears with higher intensities (Figure 3B). The elements Cu and K also appear with lower intensities. This composition is associated with the lignocellulosic structure and the plant's minerals. However, when the energy beam was positioned at point P1 in Figure 3C, chemical mapping showed increased intensities for the elements O and Si, indicating the formation of silica. Other chemical elements also exhibit lower energy intensities, such as Mg, Al, and Fe, and may be associated with the formation of oxides of these metals (Figure 3D).

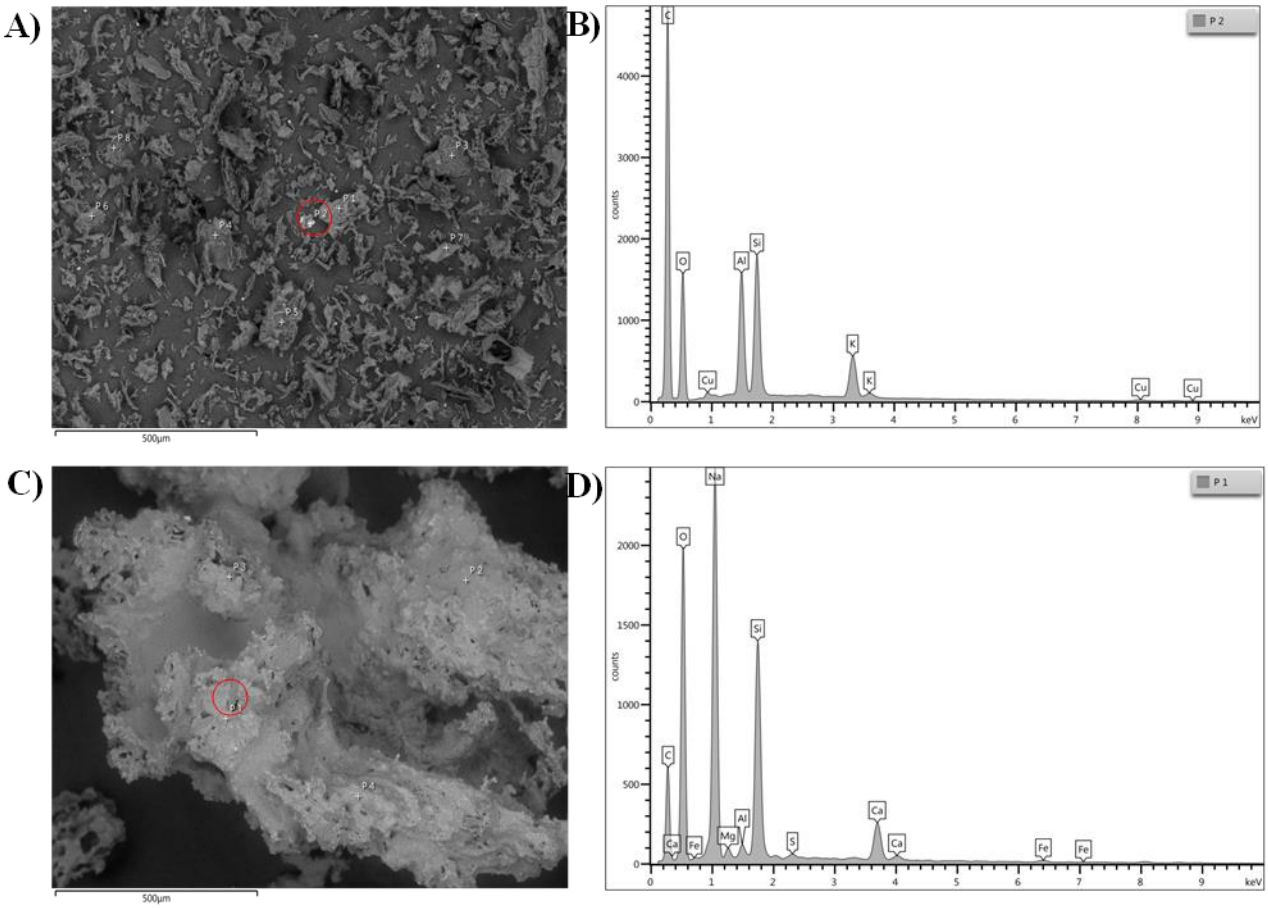

Figure 3 (A) FEG-SEM image and (B) EDS spectrum of the natural fiber. (C) FEG-SEM image and (D) EDS spectrum of the ash (SiO_2).

The synthesis of magnetic nanoparticles (Fe_3O_4) was carried out based on the coprecipitation method in the presence of silica [9], as detailed in the experimental section. Figure 4A shows photos of the final Np-Fe_3O_4/SiO_2 suspension in response to an applied external magnetic field (neodymium magnet). Within 70 seconds, all the suspended material responds to the magnetic field, indicating rapid magnetization of the nanoparticles. UV-Vis spectroscopy was used to confirm the formation of nanoparticles. Thus, Figure 4B shows the UV spectrum of the solution containing a mixture of iron (II) and iron (III) chloride salts, with an intense absorption band at nm, attributed to metal-ligand transitions [39] (red line). After the synthesis of the nanoparticles (black line), the spectrum shows a baseline evaluation due to light scattering from the nanoparticle surface, without the appearance of defined bands, which is typical of magnetite in suspension at nanometric scale. UV-Vis spectroscopy for the silica suspension (blue line) also did not reveal defined bands, as expected.

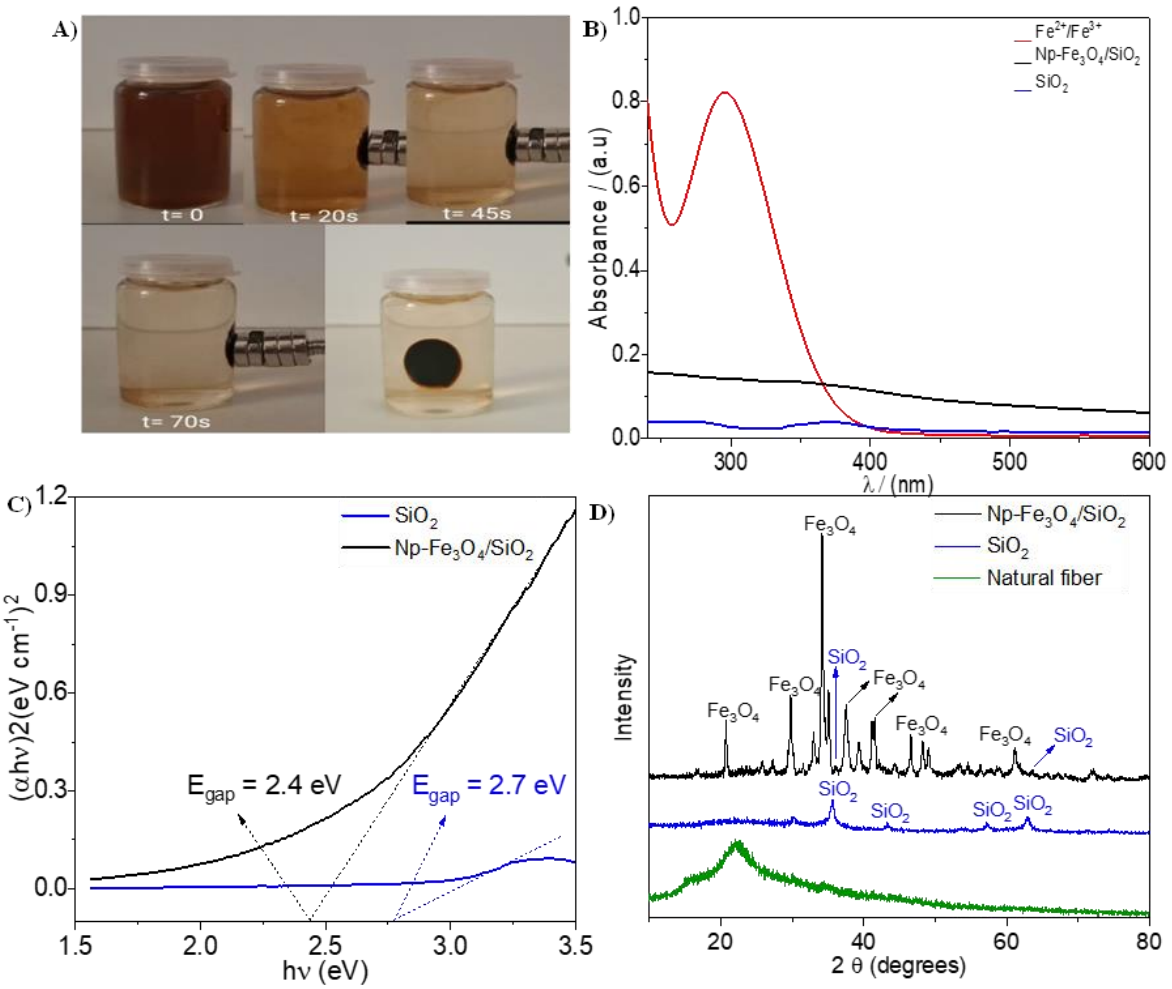

Figure 4 (A) Photographs showing the application of an external magnetic field (neodymium magnet) to the Np-Fe_3O_4/SiO_2 suspension. (B) UV-Vis spectra for SiO_2 (blue), Np-Fe_3O_4/SiO_2 suspension (black), and a mixture of $FeCl_3$ and $FeCl_2$ solutions (red). (C) Tauc plots for determining the band gap for SiO_2 (blue) and Np-Fe_3O_4/SiO_2 (black). (D) X-ray diffractograms for natural coconut (green), SiO_2 (blue), and Np-Fe_3O_4/SiO_2 (black).

In Figure 4C, the UV-Vis absorption spectra enabled us to estimate the band gap between SiO_2 and Np-Fe_3O_4/SiO_2 materials. Considering the Tauc plot (αhν × E) n, where α is the absorption coefficient, h is Planck's constant, v is the photon frequency, v is equal to 2 (direct transitions), and E is the energy in eV. Extrapolating the tangent line to the curves, we obtained the band gap energies of 2.7 eV and 2.4 eV for SiO_2 and Np-Fe_3O_4/SiO_2, respectively. The value obtained for the SiO_2 band gap may be attributed to impurities present in the silica, originating from the organic matrix of the calcined biomass, as seen in the EDS spectra in Figure 3. The decrease of 0.3 eV for the Np-Fe_3O_4/SiO_2 can be explained by the formation of a heterojunction generated in the mixed composite.

The analysis of the crystalline behavior of the materials was performed by X-ray diffraction. In Figure 4D, the diffractogram associated with the natural fiber reveals an amorphous profile (without fine peaks), showing only two peaks (2θ = 18° and 25°) of low intensity and broad base, which may be related to crystalline cellulose [40] (green line). However, the silica obtained at

800°C presents a diffractogram containing low-intensity peaks at 2θ = 35°, 43°, 57°, and 63° (blue line). The presence of these peaks indicates the presence of silica in the quartz phase. Upon forming the nanoparticles (black line), the diffractogram shows higher-intensity peaks at 2θ = 23°, 31°, 32°, 47°, 52°, and 58°. These peaks are associated with the crystalline phase of magnetite. The presence of two peaks associated with the quartz phase of silica is also noted. This behavior suggests that magnetite formed on the silica, potentially leading to phase overlap, as reported by Martins and co-workers [9].

SEM confirmed the geometry of the Np-Fe_3O_4/SiO_2 system. Figure 5A and Figure 5B show FEG-SEM images at different magnifications and zoom levels. In these two images, the nanoparticles are aggregated, approximately spherical, and average 8 nm in size. It is possible to calculate the crystallite size (D) from the Scherrer equation (Equation 2) using the highest intensity indexed peak in the nanoparticle diffractogram. By using the constant K = 0.91 (spherical particles with cubic symmetry), the X-ray wavelength (λ = 0.54 nm), the full-height peak width (FWHM) β = 1.31, and the Bragg angle (θ = 0.31), the value of 6.1 nm was obtained, a result close to the information provided by FEG-SEM.

$$D = \frac{K \times \lambda}{\beta \times \cos\cos\theta} \tag{2}$$

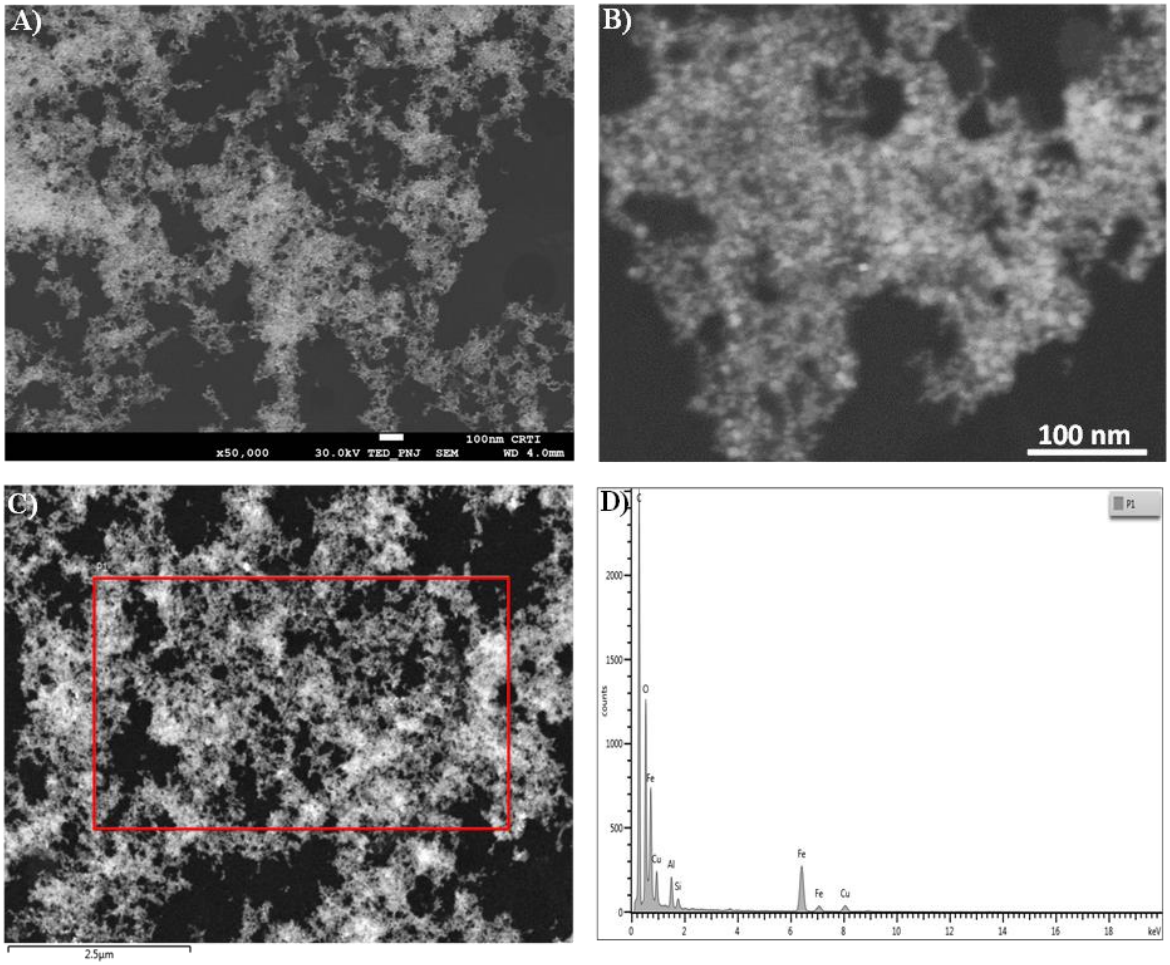

Figure 5 (A), (B), and (C) FEG-SEM images at different magnifications. (D) Chemical mapping by EDS.

The chemical mapping performed in the highlighted red region of Figure 5C revealed a chemical composition with energies associated with the chemical elements O and Fe at higher intensities, as well as energy peaks associated with the chemical elements Cu, Al, and Si at lower intensities (Figure 5D). The low peak intensity of the energy associated with silicon corroborates the information seen in the X-ray diffractogram for the Np-Fe_3O_4/SiO_2 system, in which the magnetite phase overlays the quartz phase of silica.

The suspension of nanoparticles was applied in heterogeneous photodegradation reactions of the yellow dye tartrazine. Initially, the region of greatest UV absorption for the dye was analyzed. Thus, Figure 6A shows an intense absorption band of tartrazine at 426 nm, associated with the absorption of the azo group (N=N) present in the chemical structure of the dye [9, 41], as Figure 6A shows. The photocatalytic performance of the systems Ttz + H_2O_2, Ttz + SiO_2 + H_2O_2, and Ttz + Np-Fe_3O_4/SiO_2 + H_2O_2 was evaluated using artificial UV light. Figure 6B shows the absorbance as a function of exposure time of the reaction between the materials and in the presence of hydrogen peroxide. After 75 min of reaction, the absorbances decreased from 0.3 (a.u.) to 0.2, 0.1, and 0.03, respectively, for systems Ttz + H_2O_2, Ttz + SiO_2 + H_2O_2, and Ttz + Np-Fe_3O_4/SiO_2 + H_2O_2. The photodegradation of tartrazine was also investigated in the presence of the two materials, without peroxide, as detailed in Figure 6B. In the absence of H_2O_2, the catalytic performance of the materials is less favorable for dye degradation, with degradation percentages of 4.1% for TTz + light, 6.2% for Ttz + SiO_2 + light, and 18% for Ttz + Np-Fe_3O_4/SiO_2 + light. However, the dye-degradation capacity against the Np-Fe_3O_4/SiO_2 system is three times greater and can be attributed to the increased surface area of the nanocatalyst.

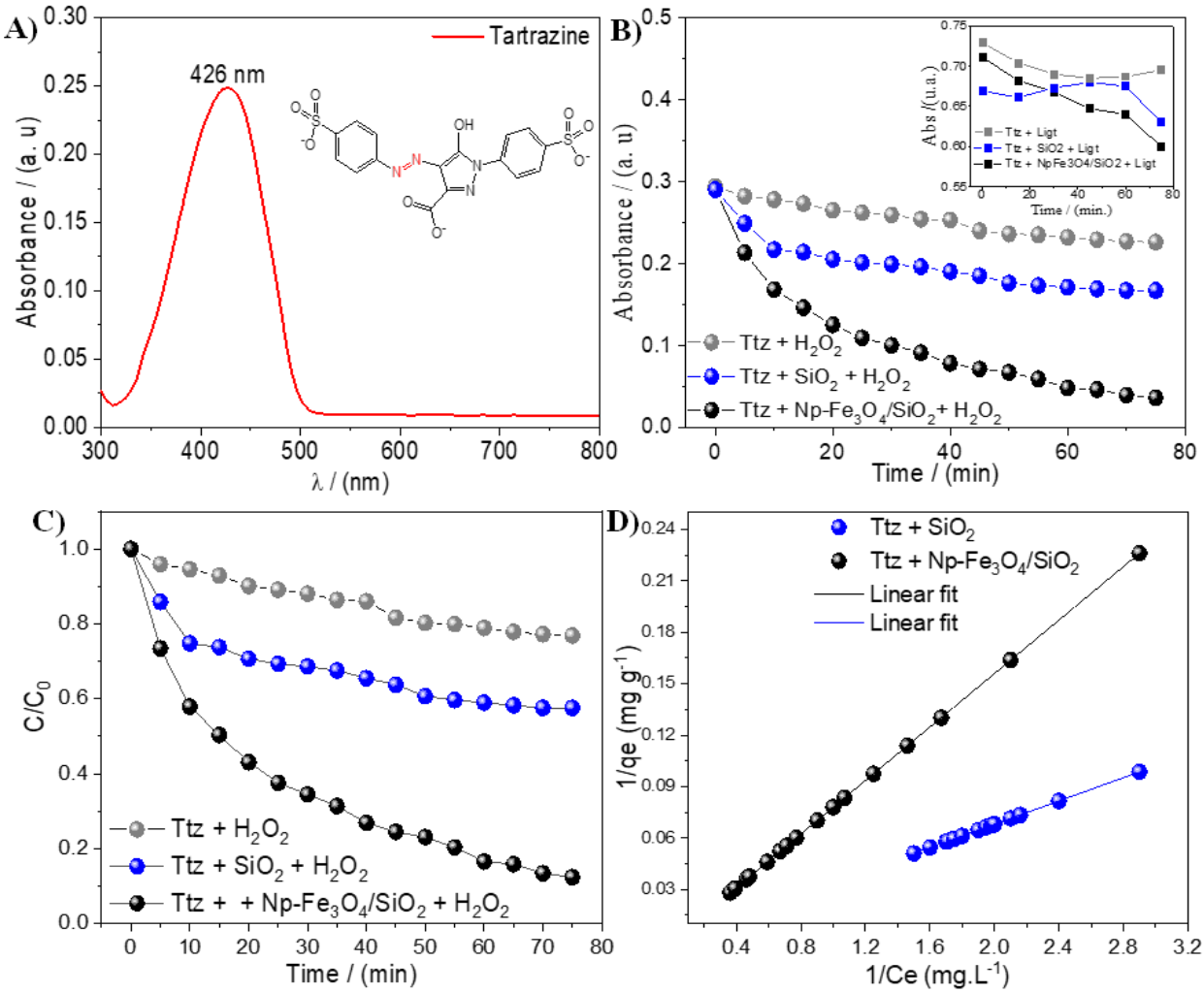

Figure 6 (A) UV-Vis spectrum for the dye TTz. (B) Abs vs. Time photodegradation spectra for Ttz + H_2O_2 (gray), Ttz + SiO_2 + H_2O_2 (blue), and Ttz + Np-Fe_3O_4/SiO_2 + H_2O_2 (black). The figure shows Abs vs. Time for the no-peroxide condition. (C) C/C_0 vs. time graph for Ttz + H_2O_2 (gray), Ttz + SiO_2 + H_2O_2 (blue), and Ttz + Np-Fe_3O_4/SiO_2 + H_2O_2 (black). (D) Graph showing the Langmuir-Hinshelwood linearization for Ttz + SiO_2 + H_2O_2 (blue) and Ttz + Np-Fe_3O_4/SiO_2 + H_2O_2 (black).

When plotting the C/C_0 ratio versus time (Figure 6C), now for photodegradation in the presence of H_2O_2, the percentage degradation values for system Ttz + H_2O_2 are 22%, for Ttz + SiO_2 + H_2O_2 are 43%, and for Ttz + Np-Fe_3O_4/SiO_2 + H_2O_2 are 91%, after 75 minutes of reaction.

In a similar study, Martins and co-authors [9] evaluated the degradation yield of tartrazine using a mixed nanomaterial composed of Fe_3O_4/SiO_2. The authors produced polymorphic nanostructures measuring 200 nm, achieving 45% dye degradation in 120 min. In contrast, this work advances the synthesis and application of the same system for the removal of tartrazine. Specifically, the nanostructures formed are approximately spherical, with a monomorphic morphology and a diameter of 8 nm. Furthermore, nearly 100% of the tartrazine is degraded at a faster rate (75 min).

The Langmuir adsorption isotherm model was used to describe the adsorption equilibrium at the interface of the photocatalysts SiO_2 and Np-Fe_3O_4/SiO_2 and the tartrazine yellow dye.

Considering that photodegradation occurs at the solid-liquid interface, the rate of tartrazine degradation depends on its adsorption/photodegradation on the surface of photocatalysts and the materials' capacity to generate e^-/h^+ pairs. Thus, the linearized Langmuir Equation 1 was used to determine these parameters. The graph in Figure 6D was obtained to depict the linearized isotherm for the reaction systems SiO_2, Np-Fe_3O_4/SiO_2, and the tartrazine yellow dye. As the experimental data (blue and black balls) follow a linear trend in the fit, this indicates that the adsorption capacities of systems SiO_2 and Np-Fe_3O_4/SiO_2 increase with increasing dye concentration. However, this increase in the adsorption capacity of tartrazine molecules is much greater when the system consisting of silica and magnetite reacts with hydrogen peroxide, which is known as the Fenton reaction. In this reaction, the magnetite surface reduces hydrogen peroxide to hydroxyl radicals, as given by Equation 3. The excess of these radicals, via photo-Fenton, accelerates the degradation of tartrazine molecules.

$$Fe^{2+} + H_2O_2 \rightarrow Fe^{3+} + HO\cdot + OH^- \quad (3)$$

The q_e values were obtained using Equation 1, and the q_m, K_L, and R_L parameters were extracted from the graph in Figure 6D and are presented in Table 2. For the Np-Fe_3O_4/SiO_2 system, these parameters are practically double when compared to the adsorption of the dye at the SiO_2 interface alone.

Table 2 Adsorption parameters.

System	Parameters			
	q_m	K_L	R_L	q_e
SiO_2	0.359	5.37	0.51	0.34
Np-Fe_3O_4/SiO_2	0.795	10.86	0.11	0.78

The Langmuir R_L parameter is a dimensionless constant, known as the separation factor, which can be used to determine whether the dye adsorption/photodegradation on the surface of adsorbents is favorable ($0 < R_L < 1$). This parameter is calculated by Equation 4.

$$R_L = \frac{1}{1 + K_L + C_0} \quad (4)$$

Based on the analysis of the kinetic parameters and photocatalytic performance, it is possible to propose a reaction mechanism for the two systems studied for the photodegradation of tartrazine in the presence of H_2O_2. When photodegradation occurs in the presence of silica, only the e^-h^+ charges generated on this surface can generate radicals ($HO^\cdot$ and $O_2^{\cdot-}$), leading to the degradation of 43% of the dye present in aqueous solution. However, in the presence of Np-Fe_3O_4/SiO_2, two factors may be at play: first, the generation of excess $HO^\cdot$ radicals via the Fenton reaction, which leads to the degradation of more dye molecules. Second, the structure of the material generated between silica and magnetite, which likely forms heterojunctions. The presence of heterojunctions [9] inhibits recombination between electrons and holes, favoring the degradation of more dye molecules, reaching up to 91%. Figure 7 is a schematic representation of this proposed photodegradation process. The advantage of this process lies in the short time it takes to virtually degrade all of the dye, the use of a magnetic photocatalyst, which allows it to be

reused, and the use of hydrogen peroxide, as it is a non-toxic molecule that degrades easily in water in the presence of magnetite.

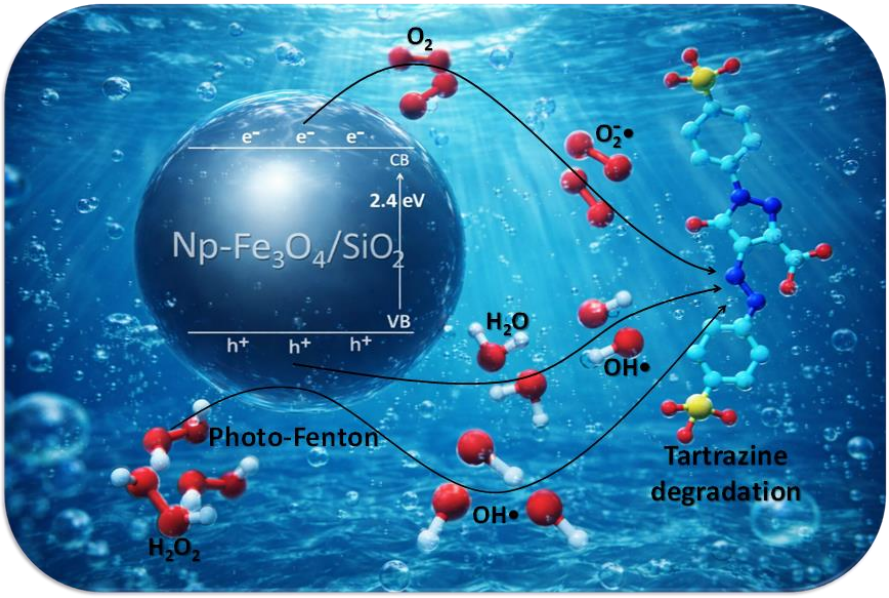

Figure 7 Schematic representation of the photodegradation process of tartrazine yellow dye at the Np-Fe_3O_4/SiO_2 interface in the presence of hydrogen peroxide.

4. Conclusions

The synthetic engineering of new materials with photocatalytic properties addresses a global need to develop and improve technologies for removing organic molecules considered pollutants in aqueous media. This study highlighted the obtaining of biosilica from coconut mesocarp, which served as a support material in the synthesis of magnetic nanoparticles. The produced nanophotocatalyst showed 18% photodegradation of the tartrazine yellow dye, which increased to almost 100% removal when the photo-Fenton reaction was used. This material is very promising because it combines decontamination characteristics, such as being removable, inexpensive, and easy to produce.

Acknowledgments

The authors express their gratitude for the scholarship funded by the Brazilian Federal Agency for Support and Evaluation of Graduate Education (CAPES Foundation).

Author Contributions

Prof. Dr. Marccus Victor Almeida Martins, marccus.victor@ifgoiano.edu.br – Obtaining experimental data, discussion of the results, preparation, and presentation of the published work. Profa. Dra. Jocélia Pereira de Carvalho Oliveira, joceliapereira@ufcat.edu.br – Discussion of the results. Profa. Dra Elaine Alves de Faria Braga, elaine.faria@ifg.edu.br – Calculation of the kinetic parameters of photodegradation and discussion of the results. Bianca Gonçalves Rodrigues, rodriguesbianca68@gmail.com – Obtaining experimental data and discussion of the results.

Competing Interests

The authors confirm that there is no conflict of interest related to the manuscript.

References

1. Deng Y, Zhao R. Advanced oxidation processes (AOPs) in wastewater treatment. Curr Pollut Rep. 2015; 1: 167-176.
2. Chen C, Ma W, Zhao J. Semiconductor-mediated photodegradation of pollutants under visible-light irradiation. Chem Soc Rev. 2010; 39: 4206-4219.
3. Thennarasu G, Rajendran S, Kalairaj A, Rathore HS, Panda RC, Senthilvelan T. A comprehensive review on the application of semiconductor nanometal oxides photocatalyst for the treatment of wastewater. Clean Technol Environ Policy. 2025; 27: 495-516.
4. Chen P, Zhai Y, Bao Y, Zhu S. Recent advances and applications of modified-semiconductor photocatalyst in pollutant degradation. In: Advances in Catalysts Research. Switzerland, Cham: Springer Nature; 2024. pp. 171-219.
5. Putul RA, Fahim SA, Masum SM, Molla MA. Fabrication and characterisation of B-ZnO nanoparticles for photodegradation of ciprofloxacin antibiotic and textile dyes. Int J Environ Anal Chem. 2025; 105: 4208-4227.
6. Pourali S, Amrollahi R, Alamolhoda S, Masoudpanah SM. In situ synthesis of ZnO/g-C_3N_4 based composites for photodegradation of methylene blue under visible light. Sci Rep. 2025; 15: 462.
7. Ali M, Gul T, Iqbal Z, Khan A, Saeed K. Photodegradation of Chlorpyrifos Pesticide by Mg Doped ZnO Nanoparticles and their Bioactivity Performance. Water Air Soil Pollut. 2026; 237: 386.
8. Rana MS, Putul RA, Salsabil N, Kabir MT, Hossain MS, Masum SM, et al. Solar-driven photodegradation of methylene blue dye using Al-doped ZnO nanoparticles. Appl Nano. 2026; 7: 3.
9. Martins MVA, Tateno NS, Brito PVR, de Carvalho Oliveira JP. Dependence of the magnetite (Fe_3O_4) and silica (SiO_2) nanostructured heterojunction for the photodegradation of tartrazine yellow dye. J Polym Sci Eng. 2025; 8: 11589.
10. Balu S, Venkatesvaran H, Wang CC, Juan JC, Yang TC. Synthesis of sulfonic acid-functionalized g-C_3N_4/BiOI bifunctional heterojunction for enhanced photocatalytic removal of tartrazine and PEC oxygen evolution reaction. Inorganics. 2024; 12: 243.
11. Luevano-Hipolito E, Sánchez-Martínez D, Juarez-Ramírez I. Pharmaceutical emerging pollutants photodegradation by the action of g-C_3N_4/$BiVO_4$ heterojunctions. Micro Nanostructures. 2025; 198: 208053.
12. Abanchime Zenaba HK, Long M, Liu X, Xu M, Luo W, et al. Electrochemical and optical insights into interfacial connection for fast pollutant removal: Experimental study of g-C_3N_4/BiOCl heterojunction for Rhb and MO photodegradation. Coatings. 2026; 16: 138.
13. Kavitha G, Govindhan M, Premkumar S. Dye pollution and its implications for human health, aquatic ecosystems, and sustainable wastewater treatment: A comprehensive review. J Water Process Eng. 2025; 80: 109071.
14. Colmenares JC, Luque R, Campelo JM, Colmenares F, Karpiński Z, Romero AA. Nanostructured photocatalysts and their applications in the photocatalytic transformation of lignocellulosic biomass: An overview. Materials. 2009; 2: 2228-2258.

15. Shabbirahmed AM, Jacob A, Dey P, Somu P, Haldar D. Biomass as eco-friendly adsorbents for the removal of emerging pollutants from wastewater: A review. Discov Appl Sci. 2025; 7: 771.
16. Fauzi AA, Chitraningrum N, Budiman I, Subyakto S, Widyaningrum BA, Maheswari CS, et al. A state-of-the-art review on lignocellulosic biomass-derived activated carbon for adsorption and photocatalytic degradation of pollutants: A property and mechanistic study. Environ Sci Pollut Res. 2024; 31: 64453-64475.
17. Shree B, Kumari S, Singh S, Rani I, Dhanda A, Chauhan R. Exploring various types of biomass as adsorbents for heavy metal remediation: A review. Environ Monit Assess. 2025; 197: 406.
18. Ghalta R, Chauhan A, Srivastava R. Heterogeneous photocatalytic valorization of lignocellulose biomass for chemical and fuel production via reductive pathways. Sustain Energy Fuels. 2024; 8: 3205-3246.
19. Fatimah I, Prakoso NI, Sahroni I, Musawwa MM, Sim YL, Kooli F, et al. Physicochemical characteristics and photocatalytic performance of TiO_2/SiO_2 catalyst synthesized using biogenic silica from bamboo leaves. Heliyon. 2019; 5: e02766.
20. El Hajam M, Kandri NI, Zerouale A, Wang X, Gustafsson J, Wang L, et al. Lignocellulosic nanocrystals from sawmill waste as biotemplates for free-surfactant synthesis of photocatalytically active porous silica. ACS Appl Mater Interfaces. 2022; 14: 19547-19560.
21. Saha A, Mishra P, Biswas G, Bhakta S. Greening the pathways: A comprehensive review of sustainable synthesis strategies for silica nanoparticles and their diverse applications. RSC Adv. 2024; 14: 11197-11216.
22. Singh G, Dizaji HB, Puttuswamy H, Sharma S. Biogenic nanosilica synthesis employing agro-waste rice straw and its application study in photocatalytic degradation of cationic dye. Sustainability. 2022; 14: 539.
23. Popoola LT, Yusuff AS, Adejare AT, Olasupo SB. Photocatalytic degradation of methylene blue dye by magnetized TiO_2-silica nanoparticles from rice husk. Appl Water Sci. 2024; 14: 25.
24. Chan AA, Buthiyappan A, Raman AA, Ibrahim S. Recent advances on the coconut shell derived carbonaceous material for the removal of recalcitrant pollutants: A review. Korean J Chem Eng. 2022; 39: 2571-2593.
25. de Almeida YA, de Fatima Gimenez I, Barreto LS, Prudente IN, dos Santos HC. Carbon-based materials from renewable sources: Challenges and perspectives with a focus on green coconut. J Chem Technol Biotechnol. 2026; 101: 477-493.
26. Hamidu I, Afotey B, Kwakye-Awuah B, Anang DA. Synthesis of silica and silicon from rice husk feedstock: A review. Heliyon. 2025; 11: e42491.
27. Yu Y, Bai X, Li S, Shi J, Wang L, Xi F, et al. Review of silicon recovery in the photovoltaic industry. Curr Opin Green Sustain Chem. 2023; 44: 100870.
28. Trukhin AN. Excitons in SiO_2: A review. J Non Cryst Solids. 1992; 149: 32-45.
29. Güler EM, Uğur GÖ, Uğur ŞU, Güler ME. A theoretical study for the band gap energies of the most common silica polymorphs. Chin J Phys. 2020; 65: 472-480.
30. Martins M, Santos TM, Faria EA, Tateno NS, Oliveira JP. Synthesis, characterization and application of magnetic nanoparticles for the photodegradation of tartrazine yellow dye. Rev Virtual Quím. 2024; 16: 740-747.
31. Khan N, Sudhakar K, Mamat R. Bio-based papers from seaweed and coconut fiber: Sustainable materials for a greener future. Carbon Resour Convers. 2025; 8: 100329.

32. Ru S, Zhang Y, Yang R, Zhang X, Yang S. Characterization based on silt retting method for extracting fibers from waste coconut husks. Ind Crops Prod. 2025; 237: 122278.
33. Salinas OA, Benítez Benítez R, Hernández FJ, Hoyos JL, Franco JM. Coconut fibers: A sustainable alternative to expanded polystyrene: A review. Cellulose. 2025; 32: 8651-8668.
34. Vieira F, Santana HE, Jesus M, Mata F, Pires P, Vaz-Velho M, et al. Comparative study of pretreatments on coconut fiber for efficient isolation of lignocellulosic fractions. Sustainability. 2024; 16: 4784.
35. Mulana F, Aulia MP, Aprilia S. Fly Ash/Coconut fiber reinforced polymer Composites: Effect on physical properties (Density, water Absorption, and thickness Swelling). Mater Today Proc. 2023; 87: 180-186.
36. Ellerbrock RH, Stein M, Schaller J. Comparing silicon mineral species of different crystallinity using Fourier transform infrared spectroscopy. Front Environ Chem. 2024; 5: 1462678.
37. Ahmad RK, Sulaiman SA, Yusup S, Dol SS, Inayat M, Umar HA. Exploring the potential of coconut shell biomass for charcoal production. Ain Shams Eng J. 2022; 13: 101499.
38. Sarker A, Rabbi AS, Nadi NA, Rahman AL, Momin AA, Ahmed KS, et al. Structural and transport properties of newly synthesized ZSM-5 sourcing silica from coconut shell ash. Results Chem. 2024; 11: 101810.
39. Dai ZY, Zhang SQ, Hong X, Wang PS, Gong LZ. A practical $FeCl_3$/HCl photocatalyst for versatile aliphatic C–H functionalization. Chem Catal. 2022; 2: 1211-1222.
40. Bichang'a DO, Oladele IO, Alabi OO, Aramide FO, Oluseye O, Borisade SG, et al. Comparative property investigation of raw and treated coconut shell biomass for potential polymer composite application. Heliyon. 2024; 10: e40704.
41. Leulescu M, Rotaru A, Pălărie I, Moanţă A, Cioateră N, Popescu M, et al. Tartrazine: Physical, thermal and biophysical properties of the most widely employed synthetic yellow food-colouring azo dye. J Therm AnalCalorim. 2018; 134: 209-231.